



# Flower-like $\text{Cr}_2\text{O}_3\text{-Cr(OH)}_3$ /poly-2-chloroaniline nanocomposite photoelectrode grown on polypyrrole film for hydrogen generation from sewage water

Amira Ben Gouider Trabelsi<sup>1</sup> · Asmaa M. Elsayed<sup>2</sup> · Fatemah H. Alkallas<sup>1</sup> · Mohamed Rabia<sup>3</sup>

Received: 3 April 2023 / Accepted: 19 August 2023 / Published online: 6 December 2023  
© The Author(s), under exclusive licence to Springer Science+Business Media, LLC, part of Springer Nature 2023

## Abstract

The flower-like  $\text{Cr}_2\text{O}_3\text{-Cr(OH)}_3$ /poly-2-chloroaniline (P2CA) nanocomposite is synthesized through oxidative polymerization of 2CA using  $\text{K}_2\text{Cr}_2\text{O}_7$ , with the preparation process performed on a polypyrrole (Ppy) seeding film. SEM images show that the P2CA material has a tissue-like structure, with fibers exhibiting a great degree of behavior. The  $\text{Cr}_2\text{O}_3\text{-Cr(OH)}_3$ /P2CA composite displays a large porous structure with flower-shaped properties and a slotted behavior, featuring circular empty holes, with nanoparticles having a pore structure ranging from 5 to 100 nm. The calculated bandgap values for P2CA and  $\text{Cr}_2\text{O}_3\text{-Cr(OH)}_3$ /P2CA are 2.02 and 1.87 eV, respectively. The  $\text{Cr}_2\text{O}_3\text{-Cr(OH)}_3$ /P2CA composite photoelectrode is utilized for hydrogen gas production from sewage water, with the produced current density ( $J_{\text{ph}}$ ) reflecting the hydrogen generation rate. The  $J_{\text{ph}}$  value in on/off light conditions demonstrates a significant enhancement under light of 0.002 and 0.018  $\text{mA}\cdot\text{cm}^{-2}$ , correspondingly. Furthermore, the  $J_{\text{ph}}$  increases from  $-0.005$  to  $-0.006$   $\text{mA}\cdot\text{cm}^{-2}$  at 340 and 730 nm, respectively, indicating the responsivity of this composite in the infrared region. So, the results demonstrate the potential of the  $\text{Cr}_2\text{O}_3\text{-Cr(OH)}_3$ /P2CA nanocomposite photoelectrode as a cost-effective and efficient alternative for the production of hydrogen gas, without the limitations associated with previous materials and techniques.

**Keywords**  $\text{Cr}_2\text{O}_3\text{-Cr(OH)}_3$  · poly-2-chloroaniline · polypyrrole · hydrogen generation · sewage water

✉ Asmaa M. Elsayed  
asmaa.elsayed@science.bsu.edu.eg

✉ Mohamed Rabia  
mohamedchem@science.bsu.edu.eg

<sup>1</sup> Department of Physics, College of Science, Princess Nourah bint Abdulrahman University, P.O. Box 84428, 11671 Riyadh, Saudi Arabia

<sup>2</sup> Physics Department, Faculty of Science, TH-PPM Group, Beni-Suef University, 62514 Beni-Suef, Egypt

<sup>3</sup> Nanomaterials Science Research Laboratory, Chemistry Department, Faculty of Science, Beni-Suef University, 62514 Beni-Suef, Egypt

## 1 Introduction

The exhaustion of natural energy resources forces researchers to find new alternative solutions. In the last decade, immense kinds of renewable energy resources have been developed, such as biomass, hydrodynamic, and solar energy (Nishiyama et al. 2021; Pagliaro 2019; T Hisatomi 2019; Takata 2020). Such resources successfully substitute natural sources and limit their hindrances. Indeed, several disadvantages of a few natural sources, like the combustion of fossil fuels, have been avoided in terms of harmful effects on plants, animals, and humans related to the intensive production of hazardous gases, such as CO<sub>x</sub>, NO<sub>x</sub>, and SO<sub>x</sub> (Asmaa M. Elsayed, Mohamed Rabia, Mohamed Shaban, Arafa H Aly 2021; Mohamed et al. 2020; Shaban et al. 2019).

Water splitting reaction becomes one of the most promising renewable solar energy routes ensuring high hydrogen production. Such energy depends mainly on sunlight effecuate through photochemical or photoelectrochemical. The source produces hydrogen gas at the working electrode. However, an appropriate semiconductor like oxides, nitrides, or sulfides is required to accomplish the splitting process. (Kang et al. 2019; Lee et al. 2018). However, these semiconductors have few hampers as photocatalytic-based material. This opens the door for researchers to develop new materials, like polymers. These latest usages ensure a cost-effective good quality, large surface, and simple synthesis way (Bec and Huck 2019; Chen et al. 2022; Kim et al. 2022; Koh et al. 2021; Yuan et al. 2020; Zhang et al. 2022).

In this regard, a good synthesis optimization of polymer material will favor its application (Rahmah 2023b; Rahmah 2023a; Rahmah et al. 2022; Rahmah and Garallah 2022; Sabry and Al-Mosawi 2017). This was realized by combining polymers with materials with high optical properties. Indeed, scientists recently succeeded in producing a material mixture of a combined material with a small bandgap of 1.3 to 2.5 eV (Shaban et al. 2017b).

Polyaniline (PANI) and its derivatives are considered one of the most investigated polymer categories so far. This polymer owns unique advantageous properties. It is known for its good stability, porosity, small bandgap, and low cost. (Abukhadra et al. 2018; Shaban et al. 2018). On the other hand, Cr<sub>2</sub>O<sub>3</sub> material proceeds with particularly promising optical and electrical properties. Also, it has a small band gap of about 1.6 to 2.5 eV, which encourages its application in various domains like optoelectronics and water splitting (Rabia et al. 2018; Shaban et al. 2017a). Nowadays, limited research is interested in polyaniline derivatives' applications in water-splitting process. Some studies prepared Ni/PANI for hydrogen gas evolution using H<sub>2</sub>SO<sub>4</sub> using artificial light (Dalla Corte et al. 2012). Furthermore, Belabed et al. (2013) had studies PANI/TiO<sub>2</sub> as a simple composite for this application. Moreover, the other literature developed PANI/MoS<sub>2</sub> for H<sub>2</sub> generation from an H<sub>2</sub>SO<sub>4</sub> solution (Zhang et al. 2015). However, several disadvantages associated with such photocatalytic polymers have been established, such as their low efficiency (2%) due to the low amount of H<sub>2</sub> formed, poor cell performance, electrode corrosion, and the destruction of natural water sources. (Acar et al. 2016; Mishra and Chun 2015; Teixeira et al. 2019). Nonetheless, the PANI material preparation method is simple and cost-effective when compared to metal oxides or sulfides material preparation methods such as vapor deposition and RF sputtering (Chiang et al. 2011; Guo et al. 2014).

Furthermore, other materials like g-C<sub>3</sub>N<sub>4</sub>-CuO (Ragupathi et al. 2020), CuO-C/TiO<sub>2</sub> (Huang et al. 2019), and TiN-TiO<sub>2</sub> (Naldoni et al. 2017) have been investigated as photoelectrodes for hydrogen generation. These studies involved measurements conducted under

strong acidic or basic conditions. However, the resulting  $J_{ph}$  values obtained from these materials were relatively low, with values of 0.01 mA.cm<sup>-2</sup>, 0.012 mA.cm<sup>-2</sup>, and 0.0003 mA.cm<sup>-2</sup>, correspondingly. These findings highlight the challenge of achieving efficient hydrogen generation using these materials in the given experimental conditions.

The materials that have been used in the past for the hydrogen gas evolution reaction have had certain limitations, such as the need for expensive techniques and additional electrolytes. These limitations have restricted the efficiency and rate of the hydrogen gas evolution reaction. However, it suggests that the Cr<sub>2</sub>O<sub>3</sub>-Cr(OH)<sub>3</sub>/P2CA nanocomposite photoelectrode overcomes these limitations, as it does not require any man-made electrolyte and can efficiently produce hydrogen gas at a high rate.

Herein, we present hydrogen gas fuel by solving polymer usage limitations. For a Cr<sub>2</sub>O<sub>3</sub>-Cr(OH)<sub>3</sub> nanocomposite prepared by polymer-assisted ionic adsorption, we used P2CA-assisted deposition; this composite is decorated over a Ppy seeding layer. The large surface area and porosity of P2CA help Cr<sub>2</sub>O<sub>3</sub> deposition. The Cr<sub>2</sub>O<sub>3</sub>-Cr(OH)<sub>3</sub>/P2CA nanocomposite photoelectrode was created by depositing the composite late into the glass. This latest was demonstrated as a photocathode in an electrochemical cell using wastewater (Beni-Suef city, Egypt). The H<sub>2</sub> gas evolution rate is evaluated through the produced  $J_{ph}$  value under various parameters such as on/off light illumination, and under monochromatic wavelengths; 340, 540, and 730 nm.

## 1.1 Materials

Pyrrole and 2-chloroaniline are obtained from Sigma Aldrich (Japan) and Merck (Germany), correspondingly. While dimethyl sulfoxide is obtained from Sigma Aldrich (USA). Winlab (UK) provides us with K<sub>2</sub>S<sub>2</sub>O<sub>8</sub>, while El Naser Co (Egypt) supplies K<sub>2</sub>Cr<sub>2</sub>O<sub>7</sub> and HCl.

## 1.2 Polypyrrole thin film' preparation

Pyrrole monomer can be oxidized and polymerized at room temperature to form polypyrrole, which has a characteristic dark green color. For performing this process, 0.12 M (0.32 ml) pyrrole is dissolved in 0.5 M hydrochloric acid. A solution of 0.15 M (1.7 g) K<sub>2</sub>S<sub>2</sub>O<sub>8</sub> is prepared separately and then added suddenly to the pyrrole solution. The stoichiometric ratio of the oxidant to monomer is 1: 1.25. This triggers the polymerization process, resulting in the formation of the dark green polypyrrole polymer. After the preparation process, we thoroughly cleaned the polymer film with distilled water and dried it at 60°C for 20 min. the polymerization reaction is mentioned in Scheme S1, while a mobile photo of polypyrrole thin film on a glass slide is illustrated in Fig. S1.

## 1.3 Cr<sub>2</sub>O<sub>3</sub>-Cr(OH)<sub>3</sub>/P2CA nanocomposite photoelectrode preparation

Cr<sub>2</sub>O<sub>3</sub>-Cr(OH)<sub>3</sub>/P2CA nanocomposite photoelectrode preparation is performed by the oxidation of 2-chloroaniline using K<sub>2</sub>Cr<sub>2</sub>O<sub>7</sub> as an oxidant. Both of monomer and the oxidant are dissolved separately in which 0.6 M HCl solution is the solvent. The greenish-brown color of the Cr<sub>2</sub>O<sub>3</sub>-Cr(OH)<sub>3</sub>/P2CA nanocomposite is formed by the reaction of K<sub>2</sub>Cr<sub>2</sub>O<sub>7</sub> and the monomer. In this reaction, the seeded polypyrrole/glass thin film is inserted into

the solution during this polymerization, this layer motivates the formation of  $\text{Cr}_2\text{O}_3\text{-Cr}(\text{OH})_3/\text{P2CA}$  nanocomposite photoelectrode.

## 1.4 Characterization and analyses

Examining the crystalline solids' structure of the materials is performed using PANalytical Pro, New Zealand, and then through the XPS analyses. Moreover, the process of determining a sample's chemical makeup using the molecular vibrations of that sample through the FTIR 340 Jasco spectrophotometer. For the morphological study, at high magnifications, SEM can provide crucial information regarding the morphology and topography of the prepared materials, ZEISS, Germany. For confirming the morphology of the sample, TEM with the JEOL JEM-2100 model is used, in which the process is performed at very high magnification. The absorbance and then bandgap calculation is performed using the UV/Vis spectrophotometer, this device has a model of Birkin Elmer, USA.

## 1.5 The electrochemical test

The behavior of the electrochemical systems is tested using the power stations (CHI608E). This process is performed by applying a potential ( $-0.85$  to  $1.1$  V) vs. RHE. Through this potential, the working electrode ( $\text{Cr}_2\text{O}_3\text{-Cr}(\text{OH})_3/\text{P2CA}$  nanocomposite photoelectrode) responds and produces the current density ( $J_{\text{ph}}$ ). In this cell, the graphite electrode functions as the counter electrode, while the calomel electrode serves as the third electrode. through which the potential inside the cell is determined. A high-intensity discharge metal halide lamp (400 W) is applied as a light source for the photocatalytic reaction. Sewage water (third treated water, pH 7.2) is used as the source of hydrogen gas, this water is applied as an electrolyte inside the cell.

# 2 Results and discussion

## 2.1 Characterization procedures

The surface topography and morphology of P2CA and  $\text{Cr}_2\text{O}_3\text{-Cr}(\text{OH})_3/\text{P2CA}$  are depicted in Fig. 1a and b, respectively, using SEM analysis, while the 2D morphologies are illustrated through TEM (Fig. 1c and d) respectively. The SEM images reveal that the P2CA material exhibits a fibrous structure, with interconnected fibers forming a network. The fibers have an average length of  $2\text{-}3$   $\mu\text{m}$  and a width of approximately  $100$  nm. This unique fibrous morphology provides a large surface area and interstitial spaces, which are advantageous for incorporating and interacting with other materials during the composite formation process.

The composite material,  $\text{Cr}_2\text{O}_3\text{-Cr}(\text{OH})_3/\text{P2CA}$ , exhibits significant improvements in its topography and morphology compared to the individual components. The addition of  $\text{Cr}_2\text{O}_3\text{-Cr}(\text{OH})_3$  to P2CA results in the formation of a highly porous structure with distinctive flower-shaped features. The material displays a slot-like behavior with circular empty holes distributed throughout its surface. These nanoparticles within the composite exhibit a pore structure ranging from  $5$  to  $100$  nm, further enhancing the material's porous nature. These unique characteristics contribute to the increased surface area and improved properties of the  $\text{Cr}_2\text{O}_3\text{-Cr}(\text{OH})_3/\text{P2CA}$  composite material. The cross section of this

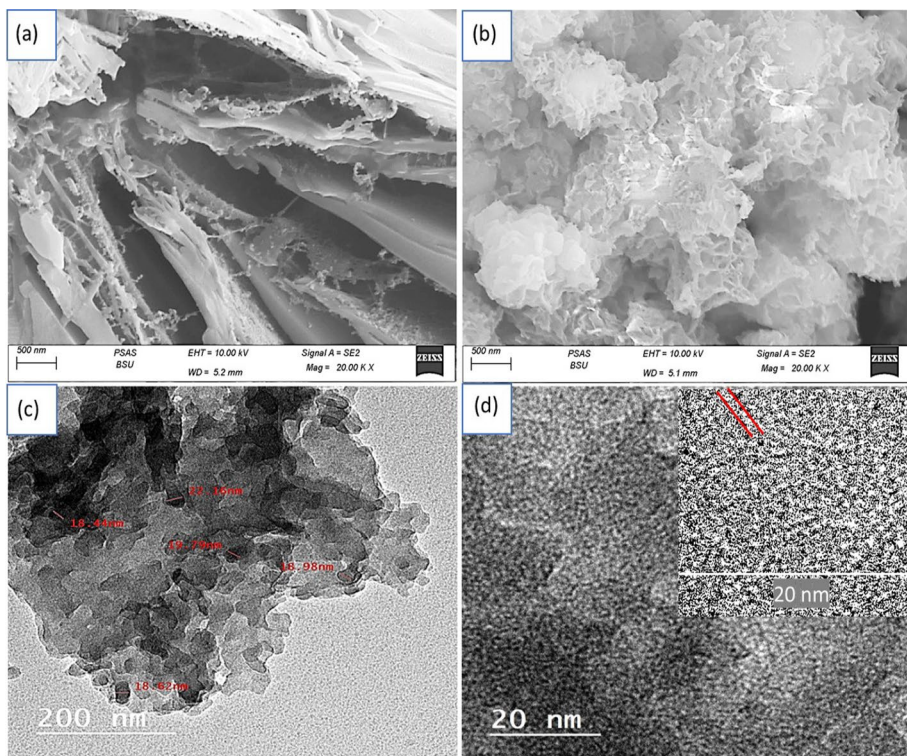


**Fig. 1** SEM of **a** P2CA, **b**  $\text{Cr}_2\text{O}_3\text{-Cr(OH)}_3/\text{P2CA}$  nanocomposite. **c** and **d** TEM of this nanocomposite at different magnifications

$\text{Cr}_2\text{O}_3\text{-Cr(OH)}_3/\text{P2CA}$  nanocomposite is mentioned in Fig. S2., which is obtained through the simulated modeling from SEM.

To be more specific, the TEM image shows the extensive incorporation of  $\text{Cr}_2\text{O}_3\text{-Cr(OH)}_3$  into the P2CA polymer materials; the metal has a dark color and an average particle size of 18 nm, while the polymer coats these particles with its gray color. Using the inserted magnified image, the interatomic distance is about 2.0 nm, illustrating the growth of the particles that order beside each other, these properties demonstrate promising optical properties

On the other hand, porous, homogeneous, semispherical particles (450 nm) make up the Ppy seeding thin film layer (Fig. S2(a)). These particles have an average size of 15 nm and are composed of numerous smaller particles that aggregate to form bigger semispherical shapes. With their wrinkled microscopic particles, the Ppy particles' shape makes them ideal for usage as a seed layer for the development of further nanomaterials. The homogeneous shape of the particles assures constant and predictable growth behavior, while the porous structure reflects the high surface area of the Ppy particles allow the nucleation and formation of new materials.

The elemental and chemical structure of the synthesized  $\text{Cr}_2\text{O}_3\text{-Cr(OH)}_3/\text{P2CA}$  nanocomposite is performed using the XRD analysis as illustrated in Fig. 2a. The P2CA polymer has an amorphous structure that appears through the broad peaks, this behavior is matched with most of the polymers that have a nanocrystalline structure (Gamal

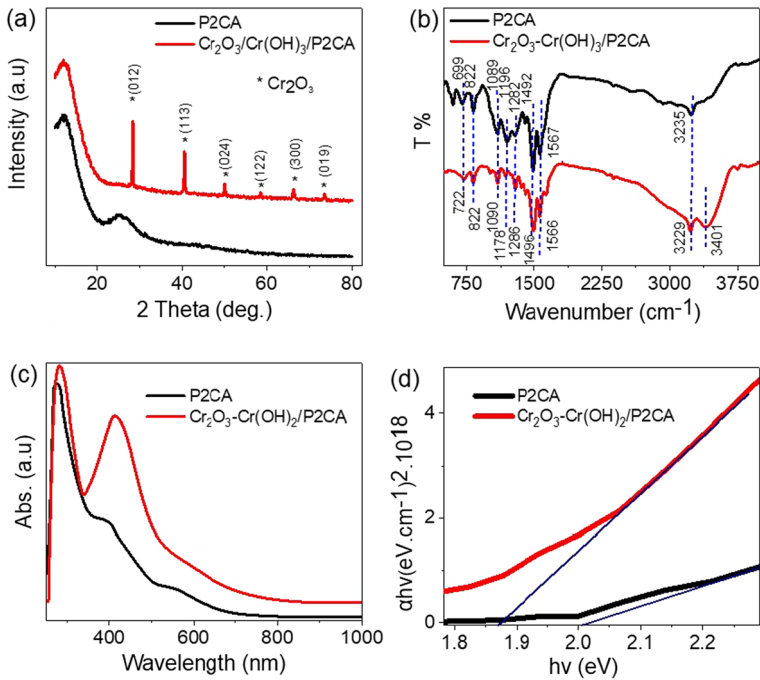


**Fig. 2** **a** XRD, **b** FTIR, **c** optical, and **d** bandgap for the P2CA and  $\text{Cr}_2\text{O}_3\text{-Cr(OH)}_3/\text{P2CA}$  nanocomposite

et al. 2022; Rabia et al. 2022). In contrast, the  $\text{Cr}_2\text{O}_3\text{-Cr(OH)}_3/\text{P2CA}$  nanocomposite exhibited a crystalline structure, as evidenced by the sharp peaks observed at certain angles:  $23.38^\circ$ ,  $40.59^\circ$ ,  $50.23^\circ$ ,  $58.67^\circ$ ,  $66.36^\circ$ , and  $73.58^\circ$ . These peaks matched with the growth directions (012), (113), (024), (122), (300), and (019), correspondingly that confirmed the presence of  $\text{Cr}_2\text{O}_3$  inside the composite (Tsegay et al. 2021). The XRD analysis does not confirm the  $\text{Cr(OH)}_3$ ; this is normal for this material and consistent with previous literature (Balayeva et al. 2019; Zhang et al. 2014).

For the calculation of the crystalline size ( $D$ ) of this composite,  $\text{Cr}_2\text{O}_3\text{-Cr(OH)}_3/\text{P2CA}$ , using the width of a crystal's diffraction ( $W$ ), Scherrer's formula, Eq. 1 (Almohammed et al. 2021; Fadel et al. 2018a) is applied, using the X-ray diffraction wavelength ( $\lambda$ ). Under these calculations, the average  $D$  size is 75 nm for the crystalline peaks located at  $40.59^\circ$  and  $66.36^\circ$ .

$$D = 0.9\lambda / W \cos\theta \quad (1)$$

The seeding Ppy layer is characterized using SEM and XRD, in which the Ppy film has porous spherical particles (Fig. S3(a)) with a semicrystalline behavior through the XRD pattern (Fig. S3(b)). The Ppy film is advantageous for supporting the growth of additional materials within the polymer network, enabling their growth and development. The FTIR analysis for this seeding layer is mentioned in Fig. S3(c). All the bands for the Ppy polymer appear, such as  $1545\text{ cm}^{-1}$  (ring), while the bands at  $1312$  and  $1177\text{ cm}^{-1}$  are for C–H, in the same way, the band at  $1045\text{ cm}^{-1}$  is for the C–N group.

FTIR analyses reveal the functional groups of the P2CA and  $\text{Cr}_2\text{O}_3\text{-Cr(OH)}_3/\text{P2CA}$  nanocomposite (Fig. 2b). N–H and C–N group appears at  $3235\text{ cm}^{-1}$  and  $1567\text{ cm}^{-1}$ ,

respectively. Also, the C-H group locates at 1492 cm<sup>-1</sup>. C=C and C-Cl groups appear well at 1282 cm<sup>-1</sup> and 699 cm<sup>-1</sup>, correspondingly. These functional groups appear in the Cr<sub>2</sub>O<sub>3</sub>-Cr(OH)<sub>3</sub>/P2CA composite, but with minor blue shifts (in most of the function groups) due to the effect of Cr<sub>2</sub>O<sub>3</sub>-Cr(OH)<sub>3</sub> inorganic materials. This behavior matches with most polymer composite (Hadia et al. 2022).

The nanocomposite made up of P2CA and Cr<sub>2</sub>O<sub>3</sub>-Cr(OH)<sub>3</sub> exhibits strong optical absorption in both the ultraviolet and visible regions, as shown in Fig. 2a and b, with absorption peaks extending up to 700 nm and 800 nm, respectively. The incorporation of Cr<sub>2</sub>O<sub>3</sub>-Cr(OH)<sub>3</sub> into the nanocomposite enhances its sensitivity to photons in the visible region, indicating its potential for use in optical applications. This enhancement is likely due to electron transitions within the nanocomposite, which motivate the observed changes in optical properties.

The optical properties of the P2CA and Cr<sub>2</sub>O<sub>3</sub>-Cr(OH)<sub>3</sub>/P2CA nanocomposite can be quantitatively described using Tauc's equations, which depend on the material's absorbance (A) and absorption coefficient (α). By applying Eqs. 2 and 3 of Tauc's equations (Fadel et al. 2018b), it is possible to calculate the bandgap of the material using these parameters. The bandgap is a characteristic property of a material that describes the electron transition process.

In Tauc's equations, h and ν are the Planck's const. and frequency. By measuring the absorbance and absorption coefficient of the nanocomposite in the UV-Vis spectra, it is possible to determine the bandgap of the material and gain further insight into its electronic properties. The observed enhancement in photon sensitivity in the Vis region may be related to reduce in the bandgap under the insertion of Cr<sub>2</sub>O<sub>3</sub>-Cr(OH)<sub>3</sub> into the nanocomposite.

$$\alpha h\nu = A(h\nu - E_g)^{1/2} \quad (2)$$

$$\alpha = \left( \frac{2,303}{d} \right) A \quad (3)$$

The bandgap confirms this enhancement as demonstrated in Fig. 2b. By calculating the bandgap using the equation  $E_g = 1240/\lambda$ , where λ is the wavelength corresponding to the absorption edge (668 nm in this case), the bandgap of the composite is determined to be approximately 1.87 eV. This indicates that the composite has a relatively low bandgap, allowing it to absorb a wide range of wavelengths in the visible and near-infrared regions. The wide optical bandgap of the Cr<sub>2</sub>O<sub>3</sub>-Cr(OH)<sub>3</sub>/P2CA nanocomposite, makes it suitable for various photocatalytic applications, such as green hydrogen generation and photovoltaic devices. This broad range of absorption allows for efficient utilization of solar energy, enabling the material to harness a wider spectrum of light for catalytic reactions or energy conversion processes. Its optical properties make it a promising candidate for sustainable energy applications.

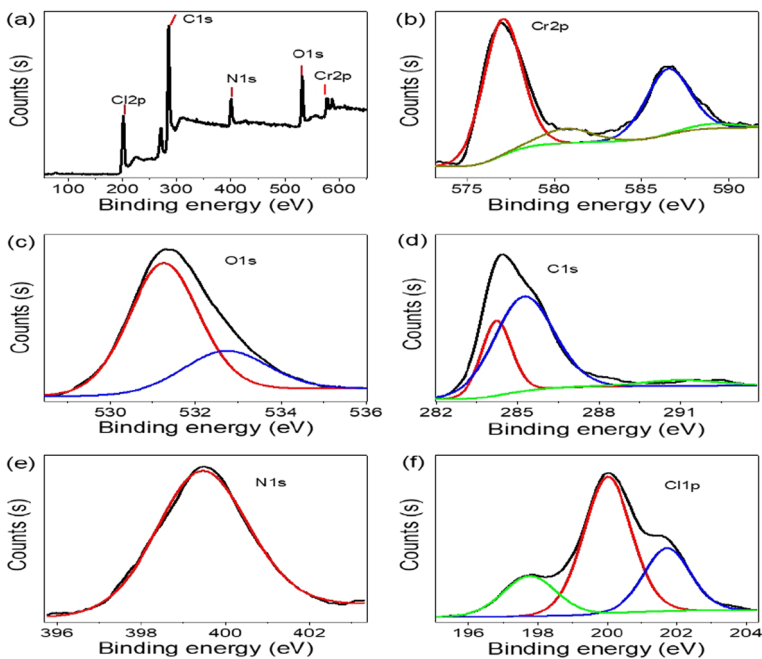
In contrast to the P2CA and Cr<sub>2</sub>O<sub>3</sub>-Cr(OH)<sub>3</sub>/P2CA nanocomposite, the optical properties of a Ppy film are limited, as shown in Fig. S3(d). The Ppy film exhibits strong absorbance in the UV region only, indicating limited sensitivity to photons in the visible range. However, this property makes Ppy film a good candidate for use as a seeding layer in the growth of the Cr<sub>2</sub>O<sub>3</sub>-Cr(OH)<sub>3</sub>/P2CA nanocomposite. The seeding layer does not significantly affect the light absorbance of the resulting nanocomposite while promoting its growth.

Figure 3a shows an XPS survey of the  $\text{Cr}_2\text{O}_3\text{-Cr(OH)}_3/\text{P2CA}$  nanocomposite. Figure 3b displays the Cr spectra, which reveal the Cr 2p<sub>3/2</sub> and 2p<sub>1/2</sub> peaks derived from  $\text{Cr}_2\text{O}_3$  and  $\text{Cr(OH)}_3$  at 577.93 and 287 eV, respectively. Additionally, Fig. 3c shows the appearance of the O1s peak at 532.31 eV, confirming the presence of oxygen in both the  $\text{Cr}_2\text{O}_3\text{-Cr(OH)}_3$  materials. The ratio of O to Cr is about 4.6, indicating the formation of oxide and hydroxide at the same time in the Cr atom (Bumajdad et al. 2017). Furthermore, different other components have been distinguished in Fig. 3d, e, and f, including C1s, Cl2p, and N1s at 285.82, 201.05, and 400.25 eV, respectively.

## 2.2 The electrochemical study

The prepared  $\text{Cr}_2\text{O}_3\text{-Cr(OH)}_3/\text{P2CA}$  nanocomposite supported on the Ppy seeding layer as a working electrode in a hydrogen generation cell that uses wastewater as an electrolyte (third treatment). Inside this cell, the graphite rod serves as a counter electrode using the CHI60E as a power station for this testing.

The great enhancement in the produced  $J_{\text{ph}}$  value under light is illustrated well in Fig. 4a, red curve. The  $J_{\text{ph}}$  value in off/on light clarifies the great enhancements under light, these values are 0.002 and 0.018  $\text{mA}\cdot\text{cm}^{-2}$ , correspondingly. The negative value of the  $J_{\text{ph}}$  indicates the reduction process and the hydrogen generation reaction, while the small dark current indicates the semiconductor nature of the synthesized  $\text{Cr}_2\text{O}_3\text{-Cr(OH)}_3/\text{P2CA}$  nanocomposite. The wide absorbing behavior of this composite, as indicated before in the optical measurements, motivates the electron transition and then the collections on the conducting band, in which these electrons transfer to



**Fig. 3** XPS a survey, b Cr, c O, d C, e N, and f Cl elements of the  $\text{Cr}_2\text{O}_3\text{-Cr(OH)}_3/\text{P2CA}$  nanocomposite



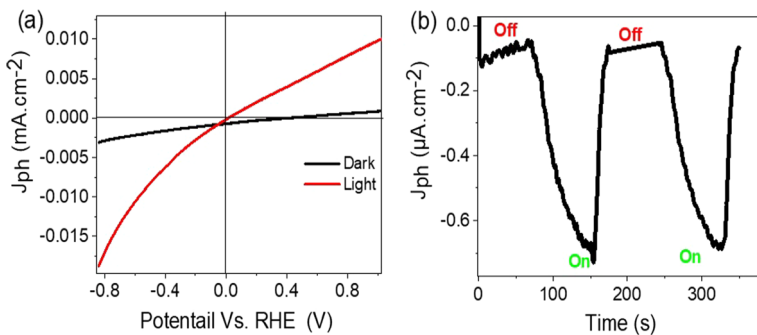


**Fig. 4** **a** The current density under the applied potential in on/off light conditions, and **b** the current density reproducibility under on/off chopped light for the working electrode Cr<sub>2</sub>O<sub>3</sub>-Cr(OH)<sub>3</sub>/P2CA nanocomposite

the neighboring solution (wastewater) for additional reduction and the hydrogen gas production. The hydrogen gas rate is represented by the  $J_{ph}$  value (Sayyah et al. 2016a; Sayyah et al. 2016b), so the rate increases well after the light illumination. The electrochemical behavior of Ppy thin film is illustrated in Fig. S4, in which the maximum  $J_{ph}$  is 0.01 mA.cm<sup>-2</sup> under light illumination.

Figure 4b shows that the Cr<sub>2</sub>O<sub>3</sub>-Cr(OH)<sub>3</sub>/P2CA nanocomposite exhibits similar behavior as the one described above, in terms of its response to on/off chopped light. This behavior indicates that the nanocomposite is highly sensitive to the incidence of photons. Furthermore, this sensitivity suggests that the nanocomposite can be reliably used for the hydrogen reduction reaction from wastewater solutions. Overall, the results from Fig. 4b provide a strong indication of the reproducibility and reliability of the Cr<sub>2</sub>O<sub>3</sub>-Cr(OH)<sub>3</sub>/P2CA nanocomposite for use in wastewater treatment applications (Table 1).

Figure 5 a and b demonstrate the sensitivity of the Cr<sub>2</sub>O<sub>3</sub>-Cr(OH)<sub>3</sub>/P2CA nanocomposite photoelectrode to different monochromatic light wavelengths, specifically 340, 540, and 730 nm. The results show that the optimum  $J_{ph}$  value is achieved at 340 nm, indicating that the nanocomposite is highly sensitive to increasing light frequency. Furthermore, the results confirm that the photoelectrode exhibits responsivity in the infrared (IR) region, as evidenced by the increase in  $J_{ph}$  from -0.005 to -0.006 mA.cm<sup>-2</sup> at 340 and 730 nm, correspondingly.

These findings demonstrate that the Cr<sub>2</sub>O<sub>3</sub>-Cr(OH)<sub>3</sub>/P2CA nanocomposite photoelectrode is sensitive to a wide range of optical frequencies, including the IR region, and suggest that the nanocomposite can significantly enhance the hydrogen reaction. Overall, the results from Fig. 5 a and b highlight the potential of the Cr<sub>2</sub>O<sub>3</sub>-Cr(OH)<sub>3</sub>/P2CA nanocomposite as an efficient and versatile material for use in a range of photoelectrochemical applications.

When a very small, applied potential of -0.1 V is used, the hydrogen reduction reaction occurs and H<sub>2</sub> gas is evolved at the cathode. This can be confirmed through the Faraday law, which is described by Eq. 4 [5]. The rate of H<sub>2</sub> gas production is about 20 μmole.h<sup>-1</sup>.10cm<sup>-2</sup> of the Cr<sub>2</sub>O<sub>3</sub>-Cr(OH)<sub>3</sub>/P2CA nanocomposite photoelectrode. The Faraday law is based on the Faraday constant (F), which has a value of 96500 C mol<sup>-1</sup>.

The high rate of hydrogen gas production observed in this study indicates the potential for industrial applications and the use of sewage water as a hydrogen source, without the need for any man-made electrolyte. Overall, these findings suggest that the

**Table 1** The concentration of the different elements and materials in the sewage water used for hydrogen generation.

Material or element	Concentration (mg/L)
Hg <sup>2+</sup>	0.005
NH <sub>3</sub>	5.0
F <sup>-</sup>	1.0
Al <sup>3+</sup>	3.0
Pesticides	0.2
NH <sub>3</sub>	5.0
Phenols	0.015
Hg <sup>2+</sup>	0.005
Cd <sup>3+</sup>	0.05
Pb <sup>2+</sup>	0.5
Cr <sup>3+</sup>	1.0
As <sup>3+</sup>	0.05
Ni <sup>3+</sup>	0.1
Cu <sup>2+</sup>	1.5
Industrial washing	0.5
Mn <sup>2+</sup>	1.0
Fe <sup>3+</sup>	1.5
Ag <sup>+</sup>	0.1
Zn <sup>2+</sup>	5.0
Co <sup>2+</sup>	2.0
Ba <sup>3+</sup>	2.0
CN <sup>-1</sup>	0.1
Other cations	0.1
Coli groups	4000/100 cm <sup>3</sup>

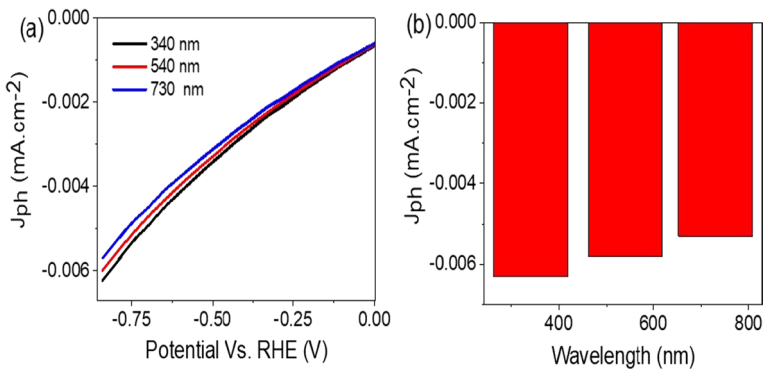


**Fig. 5** **a** The response of the fabricated Cr<sub>2</sub>O<sub>3</sub>-Cr(OH)<sub>3</sub>/P2CA nanocomposite photoelectrode to the light illumination under various optical wavelengths (340 to 730 nm) and **b** the produced J<sub>ph</sub> values under these optical filters

Cr<sub>2</sub>O<sub>3</sub>-Cr(OH)<sub>3</sub>/P2CA nanocomposite photoelectrode is a promising material for use in wastewater treatment and hydrogen gas evolution applications.

$$H_2(\text{moles}) = \int_i^t \frac{J_{ph} dt}{F} \quad (4)$$

### 3 Conclusions

A flower-like Cr<sub>2</sub>O<sub>3</sub>-Cr(OH)<sub>3</sub>/P2CA nanocomposite is synthesized by oxidation of 2CA with K<sub>2</sub>Cr<sub>2</sub>O<sub>7</sub>. The preparation process is performed on Ppy seeing film. SEM illustrates that the P2CA material has a tissue structure through the great fibers' behavior. The Cr<sub>2</sub>O<sub>3</sub>-Cr(OH)<sub>3</sub>/P2CA composite has a large porous structure with flower-shaped properties, slot behavior, and large circular empty holes, with nanoparticles with pore structures ranging from 5 to 100 nm. The calculated bandgap for P2CA and Cr<sub>2</sub>O<sub>3</sub>-Cr(OH)<sub>3</sub>/P2CA are 2.02 and 1.87 eV, respectively.

A Cr<sub>2</sub>O<sub>3</sub>-Cr(OH)<sub>3</sub>-P2CA composite photoelectrode is used to generate hydrogen from sewage water, and the produced J<sub>ph</sub> value reflects the rate of hydrogen generation. The light illumination and the optical wavelength filter condition are applied for testing the behavior of this composite. The J<sub>ph</sub> value in off/on light clarifies the great enhancements under light, these values are 0.002 and 0.018 mA.cm<sup>-2</sup>, correspondingly. Moreover, the increase in J<sub>ph</sub> from -0.005 to -0.006 mA.cm<sup>-2</sup> at 340 and 730 nm, correspondingly. These results suggest that the Cr<sub>2</sub>O<sub>3</sub>-Cr(OH)<sub>3</sub>/P2CA composite photoelectrode exhibits high sensitivity and can efficiently generate hydrogen from wastewater, making it a promising material for industrial applications.

**Supplementary Information** The online version contains supplementary material available at <https://doi.org/10.1007/s11082-023-05306-6>. Supplementary Information The online version contains supplementary material available at <https://doi.org/10.1007/s11082-023-05306-6>.

**Acknowledgments** The authors extend their appreciation to the Deputyship for Research & Innovation, Ministry of Education in Saudi Arabia for funding this research work through the project number RI-44-0689.

**Author contributions** All authors have the same contribution in this manuscript. Experimental and writing is performed by ABGT, MR, AME, and FHA, supervision and funding FHA and ABGT. All authors approve this submission.

**Funding** This research was funded by the Deputyship for Research & Innovation, Ministry of Education in Saudi Arabia through the project number RI-44-0689.

**Data availability** All data generated or analyzed during this study are included in this article.

### Declarations

**Conflict of interest** The authors declare no competing interests.

**Ethical approval** This study does not include any human or animal testings

## References

- Abukhadra, M.R., Rabia, M., Shaban, M., Verpoort, F.: Heulandite/polyaniline hybrid composite for efficient removal of acidic dye from water; kinetic, equilibrium studies and statistical optimization. *Adv. Powder Technol.* **29**, 2501–2511 (2018). <https://doi.org/10.1016/J.APT.2018.06.030>
- Acar, C., Dincer, I., Naterer, G.F.: Review of photocatalytic water-splitting methods for sustainable hydrogen production. <https://onlinelibrary.wiley.com/doi/full/10.1002/er.3549> (2016)
- Almohammed, A., Shaban, M., Mostafa, H., Rabia, M.: Nanoporous TiN/TiO<sub>2</sub>/alumina membrane for photoelectrochemical hydrogen production from sewage water. *Nanomaterials* **11**(11), 2617 (2021). <https://doi.org/10.3390/NANO11102617>
- Balayeva, O.O., Azizov, A.A., Muradov, M.B., Alosmanov, R.M., Eyvazova, G.M., Mammadyarova, S.J.: Cobalt chromium-layered double hydroxide,  $\alpha$ - and  $\beta$ - Co(OH)<sub>2</sub> and amorphous Cr(OH)<sub>3</sub>: synthesis, modification and characterization. *Heliyon* **5**, e02725 (2019). <https://doi.org/10.1016/J.HELİYON.2019.E02725>
- Bec, K.B., Huck, C.W.: Advances in near-infrared spectroscopy and related computational methods. *Molecules* **24**, 4370 (2019). <https://doi.org/10.3390/MOLECULES24234370>
- Belabed, C., Abdi, A., Benabdelghani, Z., Rekhila, G., Etxeberria, A., Trari, M.: Photoelectrochemical properties of doped polyaniline: application to hydrogen photoproduction. *Int. J. Hydrogen Energy* **38**, 6593–6599 (2013). <https://doi.org/10.1016/j.ijhydene.2013.03.085>
- Bumajdad, A., Al-Ghareeb, S., Madkour, M., Sagheer, F., Al: Non-noble, efficient catalyst of unsupported  $\alpha$ -Cr<sub>2</sub>O<sub>3</sub> nanoparticles for low temperature CO oxidation. *Sci. Rep.* **7**, 1–9 (2017). <https://doi.org/10.1038/s41598-017-14779-x>
- Chen, J., Huang, W., Zheng, D., Xie, Z., Zhuang, X., Zhao, D., Chen, Y., Su, N., Chen, H., Pankow, R.M., Gao, Z., Yu, J., Guo, X., Cheng, Y., Strzalka, J., Yu, X., Marks, T.J., Facchetti, A.: Highly stretchable organic electrochemical transistors with strain-resistant performance. *Nat. Mater.* **21**(5), 564–571 (2022). <https://doi.org/10.1038/s41563-022-01239-9>
- Chiang, C.Y., Aroh, K., Franson, N., Satsangi, V.R., Dass, S., Ehrman, S.: Copper oxide nanoparticle made by flame spray pyrolysis for photoelectrochemical water splitting: part II. Photoelectrochemical study. *Int. J. Hydrogen Energy* **36**, 15519–15526 (2011). <https://doi.org/10.1016/J.IJHYDENE.2011.09.041>
- Dalla Corte, D.A., Torres, C., Correa, P.D.S., Rieder, E.S., Malfatti, C.D.F.: The hydrogen evolution reaction on nickel-polyaniline composite electrodes. *Int. J. Hydrogen Energy* **37**, 3025–3032 (2012). <https://doi.org/10.1016/j.ijhydene.2011.11.037>
- Elsayed, A.M., Rabia, M., Shaban, M., Aly, A.H., Ahmed, A.M.: Preparation of hexagonal nanoporous Al<sub>2</sub>O<sub>3</sub>/TiO<sub>2</sub>/TiN as a novel photodetector with high efficiency. *Sci. Rep.* **11**(1), 17572 (2021)
- Fadel, M.S.S., Rabia, M., Ezzat, S., Mansour, N., Saeed, E., Sayyah, S.M.: Effect of annealing temperature on VO<sub>2</sub>(M)/ITO film nanomaterials for thermochromic smart windows application and study its contact angle. *J. Nanophotonics* **12**, 016009 (2018). <https://doi.org/10.1117/JNP.12.016009>
- Gamal, A., Shaban, M., BinSabt, M., Moussa, M., Ahmed, A.M., Rabia, M., Hamdy, H.: Facile fabrication of polyaniline/Pbs nanocomposite for high-performance supercapacitor application. *Nanomaterials* **12**, 817 (2022). <https://doi.org/10.3390/NANO12050817>
- Guo, X., Diao, P., Xu, D., Huang, S., Yang, Y., Jin, T., Wu, Q., Xiang, M., Zhang, M.: CuO/Pd composite photocathodes for photoelectrochemical hydrogen evolution reaction. *Int. J. Hydrogen Energy* **39**, 7686–7696 (2014)
- Hadia, N.M.A., Eid, S., Shaban, M., Mohamed, S.H., Elsayed, A.M., Ahmed, A.M., Alzaid, M., Abdelazez, A.A.A., El Malti, W., Rabia, M.: Poly-3-methyl aniline-assisted spherical PbS quantum dots through the ionic adsorption deposition method as a novel and highly efficient photodetector in UV, Vis, and NIR regions. *Adsorpt. Sci. Technol.* (2022). <https://doi.org/10.1155/2022/7693472>
- Hisatomi, T.: Reaction systems for solar hydrogen production via water splitting with particulate semiconductor. *Nat. Catal.* **2**, 387–399 (2019). <https://doi.org/10.1038/s41929-019-0242-6>
- Huang, X., Zhang, M., Sun, R., Long, G., Liu, Y., Zhao, W.: Enhanced hydrogen evolution from CuO<sub>x</sub>-C/TiO<sub>2</sub> with multiple electron transport pathways. *PLoS ONE* **14**, e0215339 (2019). <https://doi.org/10.1371/JOURNAL.PONE.0215339>
- Kang, Z., Cheng, Y., Zheng, Z., Cheng, F., Chen, Z., Li, L., Tan, X., Xiong, L., Zhai, T., Gao, Y.: MoS<sub>2</sub>-based photodetectors powered by asymmetric contact structure with large work function difference. *Nano-Micro Lett.* **11**, 1–12 (2019). <https://doi.org/10.1007/s40820-019-0262-4>
- Kim, D., Ndaya, D., Bosire, R., Masese, F.K., Li, W., Thompson, S.M., Kagan, C.R., Murray, C.B., Kasi, R.M., Osuji, C.O.: Dynamic magnetic field alignment and polarized emission of semiconductor nanoplatelets in a liquid crystal polymer. *Nat. Commun.* **13**, 1 (2022AD). <https://doi.org/10.1038/s41467-022-30200-2>

- Koh, Q.M., Tang, C.G., Ang, M.C.Y., Choo, K.K., Seah, Q.J., Png, R.Q., Chua, L.L., Ho, P.K.H.: Overcoming the water oxidative limit for ultra-high-workfunction hole-doped polymers. *Nat. Commun.* **12**, 1–10 (2021). <https://doi.org/10.1038/s41467-021-23347-x>
- Lee, J.H., Lee, W.W., Yang, D.W., Chang, W.J., Kwon, S.S., Park, W., Il: Anomalous photovoltaic response of graphene-on-GaN schottky photodiodes. *ACS Appl. Mater. Interfaces* **10**, 14170–14174 (2018). <https://doi.org/10.1021/acsami.8b02043>
- Mishra, M., Chun, D.M.:  $\alpha$ -Fe<sub>2</sub>O<sub>3</sub> as a photocatalytic material. A review. *Appl. Catal. A Gen.* **498**(2015), 126–141 (2015)
- Mohamed, F., Rabia, M., Shaban, M.: Synthesis and characterization of biogenic iron oxides of different nanomorphologies from pomegranate peels for efficient solar hydrogen production. *J. Mater. Res. Technol.* **9**, 4255–4271 (2020). <https://doi.org/10.1016/j.jmrt.2020.02.052>
- Naldoni, A., Guler, U., Wang, Z., Marelli, M., Malara, F., Meng, X., Besteiro, L.V., Govorov, A.O., Kildishev, A.V., Boltasseva, A., Shalaev, V.M.: Broadband hot-electron collection for solar water splitting with plasmonic titanium nitride. *Adv. Opt. Mater.* **5**, 1601031 (2017). <https://doi.org/10.1002/adom.201601031>
- Nishiyama, H., Yamada, T., Nakabayashi, M., Maehara, Y., Yamaguchi, M., Kuromiya, Y., Nagatsuma, Y., Tokudome, H., Akiyama, S., Watanabe, T., Narushima, R., Okunaka, S., Shibata, N., Takata, T., Hisatomi, T., Domen, K.: Photocatalytic solar hydrogen production from water on a 100 m<sup>2</sup> scale. *Nature* ((2021)). <https://doi.org/10.1038/s41586-021-03907-3>
- Pagliaro, M.: Preparing for the future: solar energy and bioeconomy in the United Arab Emirates. *Energy Sci. Eng.* **7**, 1451–1457 (2019). <https://doi.org/10.1002/ese3.440>
- Rabia, M., Hadia, N.M.A., Farid, O.M., Abdelazeez, A.A.A., Mohamed, S.H., Shaban, M.: Poly(m-toluidine)/rolled graphene oxide nanocomposite photocathode for hydrogen generation from wastewater. *Int. J. Energy Res.* **46**, 11943–11956 (2022). <https://doi.org/10.1002/ER.7963>
- Rabia, M., Mohamed, H.S.H., Shaban, M., Taha, S.: Preparation of polyaniline/PbS core-shell nano/microcomposite and its application for photocatalytic H<sub>2</sub> electrogeneration from H<sub>2</sub>O. *Sci. Rep.* **8**(1), 1107 (2018)
- Ragupathi, V., Raja, M.A., Panigrahi, P., Ganapathi Subramaniam, N.: CuO/g-C<sub>3</sub>N<sub>4</sub> nanocomposite as promising photocatalyst for photoelectrochemical water splitting. *Optik* **208**, 164569 (2020). <https://doi.org/10.1016/j.jlleo.2020.164569>
- Rahmah, M.I.: Novel triple hydrothermal method for preparation of CuO/Fe<sub>2</sub>O<sub>3</sub>/Ag<sub>2</sub>O nanocomposite with antimicrobial application. *Inorg. Nano-Met. Chem.* (2023). <https://doi.org/10.1080/24701556.2023.2165680>
- Rahmah, M.I.: Study the effect of graphene and silver nanoparticles on the structural, morphological, optical, and antibacterial properties of commercial titanium oxide. *Inorg. Chem. Commun.* **149**, 110441 (2023). <https://doi.org/10.1016/j.inoche.2023.110441>
- Rahmah, M.I., Garallah, E.T.: Preparation of copper oxides/polyvinyl alcohol nanocoatings with antibacterial activity. *Chem. Data Collect.* **39**, 100869 (2022). <https://doi.org/10.1016/j.cdc.2022.100869>
- Rahmah, M.I., Sabry, R.S., Aziz, W.J.: Preparation and antibacterial activity of superhydrophobic modified ZnO/PVC nanocomposite. *J. Bionic Eng.* **19**, 139–154 (2022). <https://doi.org/10.1007/S42235-021-00106-8/FIGURES/17>
- Sabry, R.S., Al-Mosawi, M.I.: Novel approach to fabricate a stable superhydrophobic polycarbonate. *Surf. Eng.* **34**, 151–157 (2017). <https://doi.org/10.1080/02670844.2016.1270620>
- Sayyah, S.M., Shaban, M., Rabia, M.: A sensor of m-toluidine/m-cresol polymer film for detection of lead ions by potentiometric methods. *Sens. Lett.* **14**, 522–529 (2016). <https://doi.org/10.1166/sl.2016.3656>
- Sayyah, S.M., Shaban, M., Rabia, M.: A high-sensitivity potentiometric mercuric ion sensor based on m-toluidine films. *IEEE Sens. J.* **16**, 1541–1548 (2016). <https://doi.org/10.1109/JSEN.2015.2505313>. ((b))
- Shaban, M., Abukhadra, M.R., Rabia, M., Elkader, Y.A., Abd El-Halim, M.R.: Investigation the adsorption properties of graphene oxide and polyaniline nano/micro structures for efficient removal of toxic Cr(VI) contaminants from aqueous solutions; kinetic and equilibrium studies. *Rend. Lincei.* **29**, 141–154 (2018). <https://doi.org/10.1007/s12210-018-0673-z>
- Shaban, M., Ali, S., Rabia, M.: Design and application of nanoporous graphene oxide film for CO<sub>2</sub>, H<sub>2</sub>, and C<sub>2</sub>H<sub>2</sub> gases sensing. *J. Mater. Res. Technol.* **8**(5), 4510–4520 (2019). <https://doi.org/10.1016/j.jmrt.2019.07.064>
- Shaban, M., Rabia, M., El-Sayed, A.M.A., Ahmed, A., Sayed, S.: Photocatalytic properties of PbS/graphene oxide/polyaniline electrode for hydrogen generation. *Sci. Rep.* **7**, 1–13 (2017). <https://doi.org/10.1038/s41598-017-14582-8>

- Shaban, M., Rabia, M., Fathallah, W., El-Mawgoud, N.A., Mahmoud, A., Hussien, H., Said, O.: Preparation and characterization of polyaniline and Ag/ polyaniline composite nanoporous particles and their anti-microbial activities. *J. Polym. Environ.* (2017). <https://doi.org/10.1007/s10924-017-0937-1>
- Takata, T.: Photocatalytic water splitting with quantum efficiency of almost unity. *Nature* **581**, 411–414 (2020). <https://doi.org/10.1038/s41586-020-2278-9>
- Teixeira, G.F., Silva Junior, E., Vilela, R., Zaghete, M.A., Colmati, F.: Perovskite structure associated with precious metals: influence on heterogenous catalytic process. *Catalysts* **9**, 721 (2019). <https://doi.org/10.3390/catal9090721>
- Tsegay, M.G., Gebretinsae, H.G., Nuru, Z.Y.: Structural and optical properties of green synthesized Cr2O3 nanoparticles. *Mater. Today Proc.* **36**, 587–590 (2021). <https://doi.org/10.1016/J.MATPR.2020.05.503>
- Yuan, C., Zhou, Y., Zhu, Y., Liang, J., Wang, S., Peng, S., Li, Y., Cheng, S., Yang, M., Hu, J., Zhang, B., Zeng, R., He, J., Li, Q.: Polymer/molecular semiconductor all-organic composites for high-temperature dielectric energy storage. *Nat. Commun.* **11**(11), 1–8 (2020). <https://doi.org/10.1038/s41467-020-17760-x>
- Zhang, N., Ma, W., Wu, T., Wang, H., Han, D., Niu, L.: Edge-rich MoS2 nanosheets rooting into polyaniline nanofibers as effective catalyst for electrochemical hydrogen evolution. *Electrochim. Acta* **180**, 155–163 (2015). <https://doi.org/10.1016/J.ELECTACTA.2015.08.108>
- Zhang, Q., Parimoo, H., Martel, E., Zhao, S.: Vertical semiconductor deep ultraviolet light emitting diodes on a nanowire-assisted aluminum nitride buffer layer. *Sci. Rep.* **12**, 1–7 (2022). <https://doi.org/10.1038/s41598-022-11246-0>
- Zhang, W., Yang, Y., Li, F., Song, G., Shao, Y., Ouyang, R., Xu, L., Li, W., Miao, Y.: A newly prepared Ni(OH)2@Cr(OH)3 nanohybrid for its bioelectrocatalysis. *Sens. Actuators B* **198**, 350–359 (2014). <https://doi.org/10.1016/J.SNB.2014.03.081>

**Publisher's Note** Springer Nature remains neutral with regard to jurisdictional claims in published maps and institutional affiliations.

Springer Nature or its licensor (e.g. a society or other partner) holds exclusive rights to this article under a publishing agreement with the author(s) or other rightsholder(s); author self-archiving of the accepted manuscript version of this article is solely governed by the terms of such publishing agreement and applicable law.